New Phytologist

REVEILLE2 thermosensitive splicing: a molecular basis for the integration of nocturnal temperature information by the Arabidopsis circadian clock

Allan B. James[1] iD, Chantal Sharples[1,2] iD, Janet Laird[1] iD, Emily May Armstrong[1] iD, Wenbin Guo[3] iD, Nikoleta Tzioutziou[4,5] iD, Runxuan Zhang[3] iD, John W. S. Brown[4,5] iD, Hugh G. Nimmo[1] iD and Matthew A. Jones[1] iD

[1]School of Molecular Biosciences, University of Glasgow, Glasgow, G12 8QQ, UK; [2]RNA Biology and Molecular Physiology, Faculty for Biology, Bielefeld University, Universitaetsstrasse 25, 33615, Bielefeld, Germany; [3]Information and Computational Sciences, The James Hutton Institute, Invergowrie, Dundee, DD2 5DA, UK; [4]Plant Sciences Division, College of Life Sciences, University of Dundee, Invergowrie, Dundee, DD2 5DA, UK; [5]Cell and Molecular Sciences, The James Hutton Institute, Invergowrie, Dundee, DD2 5DA, UK

Summary

- Cold stress is one of the major environmental factors that limit growth and yield of plants. However, it is still not fully understood how plants account for daily temperature fluctuations, nor how these temperature changes are integrated with other regulatory systems such as the circadian clock.
- We demonstrate that *REVEILLE2* undergoes alternative splicing after chilling that increases accumulation of a transcript isoform encoding a MYB-like transcription factor. We explore the biological function of *REVEILLE2* in *Arabidopsis thaliana* using a combination of molecular genetics, transcriptomics, and physiology.
- Disruption of *REVEILLE2* alternative splicing alters regulatory gene expression, impairs circadian timing, and improves photosynthetic capacity. Changes in nuclear gene expression are particularly apparent in the initial hours following chilling, with chloroplast gene expression subsequently upregulated.
- The response of *REVEILLE2* to chilling extends our understanding of plants immediate response to cooling. We propose that the circadian component *REVEILLE2* restricts plants responses to nocturnal reductions in temperature, thereby enabling appropriate responses to daily environmental changes.

Introduction

Light and temperature provide an abundance of information that enable plants to coordinate their development with available resources. Importantly, both environmental cues are highly dynamic, with daily and seasonal patterns that can provide a 'time-of-day' context in addition to reporting prevailing environmental conditions. Deciphering this temporal information requires the integration of light and temperature signals with the circadian system, which provides an endogenous timing reference. Biological timekeeping in this way contributes to numerous plant behaviors, ranging from the modulation of immediate responses to environmental signals (also known as circadian 'gating') through to significant developmental responses including flowering time (Millar, 2016).

Although light and temperature are covarying environmental cues, our understanding of plants responses to thermal cues greatly trails our understanding of photobiology, in part because many enzymatic reactions are temperature-dependent (Kerbler &

Wigge, 2023). Within minutes of exposing Arabidopsis plants to low temperature, changes in transcript accumulation can be detected followed by waves of changes in transcriptome composition (Fowler & Thomashow, 2002; Maruyama *et al.*, 2004; Vogel *et al.*, 2005). Induction of the transcriptional activators *C-REPEAT-BINDING FACTOR (CBF)1*, *-2* and *-3* (also known as *DEHYDRATION-RESPONSIVE ELEMENT-BINDING FACTOR (DREB)1b*, *-1c* and *-1a*, respectively) occurs within 15 min of low-temperature exposure with these genes inducing expression of many cold-induced genes (Chinnusamy *et al.*, 2007). Since all three *CBF* genes are rapidly and significantly induced by cold stress, their induction is generally considered to be the first switch in the cold-responsive expression of numerous genes (Yamaguchi-Shinozaki & Shinozaki, 1994; Kidokoro *et al.*, 2020). Importantly, cold induction of the *CBFs* is gated by the circadian clock, with the morning-phased circadian proteins CIRCADIAN CLOCK ASSOCIATED 1 (CCA1) and LATE ELONGATED HYPOCOTYL (LHY) promoting *CBF* expression during the day (Fowler *et al.*, 2005; Dong *et al.*, 2011).

CCA1 and LHY belong to the REVEILLE (RVE) family of proteins, all of which contain a single DNA-binding Myb-like domain that is necessary for biological function (Gray *et al.*, 2017). Other family members include RVE1 through RVE8, in addition to a RVE7-like protein. REVEILLEs appear to play contrasting roles in controlling the pace of the circadian clock; mutations in *CCA1* and *LHY* accelerate clock pace (Schaffer *et al.*, 1998; Wang & Tobin, 1998; Green & Tobin, 1999; Mizoguchi *et al.*, 2002), while disruptions in *RVE8*, *6* and *4* loci lengthen circadian period (Farinas & Mas, 2011; Rawat *et al.*, 2011; Hsu *et al.*, 2013). RVE5 and RVE3 display more subtle effects on setting the tempo of the clock (Gray *et al.*, 2017), and RVE1 does not affect clock pace but instead mediates the circadian regulation of the auxin pathway (Rawat *et al.*, 2009). By contrast, constitutive expression of either RVE2 or RVE7 has previously been reported to repress circadian gene expression (Kuno *et al.*, 2003; Zhang *et al.*, 2007). More recent work has revealed that RVE4 and RVE8 contribute to cold-induced gene expression, demonstrating how RVE proteins contribute toward the integration of temperature signals into the circadian system (Kidokoro *et al.*, 2021, 2023).

Despite the contribution of the RVE family to circadian timing, it remains unclear how temperature alters the abundance or function of these proteins. Ultra-deep RNA-sequencing (RNA-seq) of a diel time-course of plants exposed to low temperature describes *c.* 900 transcripts that are alternatively spliced after cooling, including within the 5′ UTR of *LHY* and within the coding sequence of *CCA1* (Seo *et al.*, 2012; Calixto *et al.*, 2018; James *et al.*, 2018). However, both of these alternative splicing events are likely indirect consequences of chilling since they occur several hours after the temperature change (Calixto *et al.*, 2018). We were interested whether alternative splicing events within other *RVE* transcripts had a more immediate effect upon protein function.

Here, we report alternative splicing of the *RVE2* transcript that is induced within 20 min of chilling. A T-DNA insertional mutant (*rve2-2*) that is devoid of the predominant *RVE2* isoforms displays increased accumulation of key regulatory transcripts including *CBFs*. *rve2-2* seedlings have impaired circadian rhythms at reduced temperatures and temporal profiling shows most Differentially Expressed Genes (DEGs) comprise a wave of gene expression initiated shortly after peak RVE2 expression during transient cool nights. However, we also identified a group of chloroplast-encoded genes that are repressed in *rve2-2* plants following the initial DEGs. Changes in chloroplast gene expression are correlated with altered photosynthetic capacity the following morning. Our data therefore suggest that *RVE2* represses the induction of low temperature responses during the night to enable an appropriate photosynthetic and cold-response strategy aligned with the promise of the ensuing dawn.

Materials and Methods

Plant material and growth conditions

All plant material was derived from the *Arabidopsis thaliana* (Columbia; Col-0) ecotype (Scholl *et al.*, 2000). The *rve2-1* allele has

previously been reported (Zhang *et al.*, 2007), and the *rve2-2* mutant was obtained from GABI-Kat (Kleinboelting *et al.*, 2012). *rve2-1* and *rve2-2 CCA1::LUC2* lines were generated by crossing each allele with a *CCA1::LUC2* reporter line (Jones *et al.*, 2015). The *RVE2::RVE2:LUC* construct was created by cloning the *RVE2* locus (including 1000 bp upstream of the start codon) into pDONR221 before transfer into pGWB535 using Gateway cloning (Invitrogen). *RVE2::RVE2:LUC* was transformed into *rve2-2* seedlings using agrobacteria-mediated transformation (Clough & Bent, 1998).

DNA & RNA extraction, cDNA synthesis, RT-PCR, and qPCR

RNA extraction, cDNA synthesis, and qPCR (RT-qPCR) were performed essentially as described previously (James *et al.*, 2018). Total RNA was extracted with the RNeasy Plant Mini kit (Qiagen) and Dnase treated (DNA-free; Ambion). Complementary DNA (cDNA) was typically synthesized from 2 μg of total RNA using oligo dT primers and SuperScriptII reverse transcriptase (Thermo-Fisher Scientific, Altrincham, UK). qPCRs (1 : 100 dilutions of cDNA) were performed with Brilliant III SYBR Green QPCR Master Mix (Agilent, Stockport, UK) on a StepOnePlus (Fisher Scientific-UK Ltd, Loughborough, UK) real-time PCR system. The average C_t values for *ISU1* (At4g22220) and *IPP2* (At3g02780) were used as internal control expression levels. For genotype analyses, DNA was extracted from frozen shoot tissue with the Dneasy Plant Mini Kit (Qiagen). RT-PCR was performed using cDNAs and GoTaq Green DNA polymerase (Promega). All primer sequences are provided in Supporting Information Table S1.

RNA-seq

Seeds were surface-sterilized with 3.5% NaOCl and 0.01% Triton X-100 and washed in sterile distilled H_2O followed by stratification for 2–3 d in darkness at 4°C. All plants were grown hydroponically (Tzioutziou *et al.*, 2022) in environmentally controlled growth cabinets (Microclima, Snijders Labs, Tilburg, the Netherlands). White light intensity ($100 \pm 20 \mu E\ m^{-2}\ s^{-1}$) was provided by Sylvania Grolux F36W/GRO fluorescent tubes. All plants were harvested 5 wk after sowing. Tissue was immediately frozen in liquid nitrogen and stored at −80°C until further use. Growth conditions for the RNA-seq experiments are described in Calixto *et al.* (2018). Briefly, plants were harvested at the indicated time points, with chilling to 4°C always initiated at dusk. Lighting and temperature conditions are indicated in each figure. In all cases, a single biological replicate consisted of 9–13 plants in hydroponic containers, aerial tissue harvested and pooled per condition/time point. Three biological replicates were generated for each time point in separate experiments. The same growth cabinet was used for all repeats to eliminate the potential effects of minor changes in light intensities and light quality on gene expression. Hydroponic containers were selected randomly from the growth cabinet during time series experiments to minimize biases toward growth cabinet microclimates.

Different RNA-seq experiments were performed or re-analyzed in the course of this study. First, Col-0 plants at 20°C and 4°C

were compared in a time-series covering only the first 3 h of cold treatment, referred to as the 'Immediate-Early' (IE) time-series (Dataset S1). It consisted of a total of 13 time point samples with four biological repeats. Second, we re-analyzed a previous RNA-seq dataset to compare magnitude of differential expression and differential alternative splicing (Calixto *et al.*, 2018; Dataset S2). Third, RNA-seq was conducted on Col-0 plants at 20°C and 12°C where plants were transferred to 12°C in constant light conditions. This experiment consisted of samples taken at 16 time points at 20°C and 12°C each with three biological replicates and was referred to as the 'CoolLL' time-series (Dataset S3). Finally, Col-0 and *rve2-2* plants were directly compared using the same time-series structure as described in Calixto *et al.* (2018) comparing 5-wk-old plants grown at 20°C throughout or transferred to 4°C. The experiment consisted of 26 time points each with three biological replicates (Methods S1; Dataset S4).

RNA-seq libraries were constructed using the Illumina TruSeq library preparation protocol. Libraries had an average insert size of 280 bp and were sequenced three times on the Illumina HiSeq 2500 platform to generate 100 bp paired end reads. After standard quality control and trimming of reads, transcript expression was determined using SALMON v.0.82 (Patro *et al.*, 2017) in conjunction with AtRTD2-QUASI (Zhang *et al.*, 2017).

Parameters for expression were established using Mean–Variance Trend Plots and the RNA-seq data quality was checked with principal component analysis (PCA) plot and sample distribution plot by using the 3D RNA-seq App (Guo *et al.*, 2021) and shown for Dataset S4. The RNA-seq experiments were analyzed for differential gene and transcript expression, differential alternative splicing and differential transcript usage using 3D RNA-seq as described in detail in Guo *et al.* (2021) and the 3D RNA-seq App (https://ics.hutton.ac.uk/3drnaseq). In addition, for the comparison of Col-0 with *rve2-2*, differential expression analysis of the RNA-seq data focused on the Day 2 transient-cooling data. For this dataset, low expressed genes (those with a cumulative TPM < 80 across the time points for Day 2) were filtered to increase statistical power. Transcript isoforms were considered differentially expressed if the difference between Col-0 and *rve2-2* was at least 1.2-fold for three contiguous time points. Analysis of variance (ANOVA) was used to test the variance in the RNA-seq TPM values on the explanatory factors genotype and time. The ANOVA function in the CAR (Companion to Applied Regression) package (v.3.1-1) in R was used to prepare the type-II ANOVA tables for the differentially expressed candidates (Table S2). Fisher's exact test for testing the null of independence of rows and columns in a contingency table with fixed marginals were performed in R using the fisher.test function in the 'stats' package (The R STATS Package, v.4.2.2). Other analyses and visualizations of data were carried out using the GGPLOT2 package (v.3.4.1; Wickham, 2016) in R v.4.2.2 (2022-10-31). Hutcheson's *t*-test was used to compare differences in Shannon's diversity index (Hutcheson, 1970).

GO term enrichment analysis

The Gene Ontology (GO) over-representation test (Boyle *et al.*, 2004) was implemented in clusterProfiler (Yu *et al.*, 2012) using the parameters pAdjustMethod = 'BH', pvalueCutoff = 0.05, qvalueCutoff = 0.1.

Promoter enriched motif analysis

HOMER v.4.11 was used to identify *de novo* motifs enriched in the promoters of DEGs (Heinz *et al.*, 2010). A 1000 bp sequence upstream of each genes start codon was assessed for motifs between 6 and 12 bases in length.

Chlorophyll fluorescence

Chlorophyll fluorescence parameters were recorded with a Walz IMAGING-PAM Maxi chlorophyll fluorescence system, essentially as previously described (Litthauer *et al.*, 2015). Approximately 30 individually spaced seedlings were entrained for 12 d in 12 h : 12 h, light : dark cycles on half-strength Murashige and Skoog (MS) medium without supplemental sucrose for 12 d before transfer to the imaging chamber. After transfer from the growth chamber plants were dark adapted for 30 min before determination of F_v/F_m at ZT2. At the following dusk, plants were chilled to 4°C, and then maintained at 4°C for the remainder of the experiment. Plants were dark-adapted for 30 min before determination of F_v/F_m at ZT2. A two-way ANOVA was implemented to compare genotypes at each temperature, with Tukey's multiple comparison test used to determine statistical significance. Data are representative of three independent experiments.

Luciferase imaging

Plants were entrained for 6 d in 12 h : 12 h l/D cycles under white light on MS medium without sucrose before being sprayed with 3-mM D-luciferin in 0.01% (v/v) Triton X-100 as previously described (Battle & Jones, 2020). Imaging was completed over 5 d using a Teledyne Photometrics LUMO camera controlled by µManager (Edelstein *et al.*, 2014) before data were processed using IMAGEJ (Schneider *et al.*, 2012).

Circadian parameter estimation

Patterns of luciferase activity, qRT-PCR data, and RNAseq data (for individual candidate transcripts) were fitted to cosine waves using fast Fourier transform–nonlinear least squares to estimate circadian period length using BIODARE (Zielinski *et al.*, 2014). Circadian period estimates utilized data beginning at ZT24.

Results

Nocturnal chilling induces rapid changes in patterns of *RVE2* alternative splicing

We previously identified genes which were differentially expressed (DE) and/or differentially alternatively spliced (DAS) in an extended RNA-seq time series experiment of Arabidopsis plants exposed to low temperature (Calixto *et al.*, 2018). To further understand transcriptomic changes that occur immediately

after chilling, we completed an additional RNA-seq experiment, also chilling at dusk but concentrated upon the first 3 h of cooling (Fig. 1a; Dataset S1). We quantified transcript abundance in transcripts per million (TPM) using SALMON (Patro *et al.*, 2017) and AtRTD2 as the reference transcriptome (Zhang *et al.*, 2017), allowing us to determine patterns of expression at the individual transcript isoform level for the entire transcriptome (Dataset S1). Analysis of 1286 genes that are DAS across the first 3 h of cooling in this latter RNA-seq dataset identifies two genes that are DAS (yet not DE) within the first 20 min of chilling; UBN1 (AT1G21610) and RVE2 (At5g37260, also known as CIRCA-DIAN1 (CIR1); Zhang *et al.*, 2007). UBN1 is expressed at low levels, and chilling-induced DAS does not alter the alternatively spliced isoforms that encode the UBN1 protein (Fig. S1a). By contrast, RVE2 is one of the most highly expressed genes that undergoes chilling-induced DAS (Fig. 1b; Dataset S2). Given the magnitude and speed with which RVE2 is alternatively spliced we were interested whether this DAS had functional consequences for the RVE2 protein.

Alternative splicing of RVE2 pre-mRNA generates seven different transcripts, of which only one (FS(.1)) encodes a protein containing the MYB domain necessary for DNA binding (Fig. 1c; Seo *et al.*, 2012, Zhang *et al.*, 2017, Calixto *et al.*, 2018). The other isoforms are likely nonfunctional since they encode transcripts with a premature termination codon (PTC) after either 4 or 23 amino acids, before the MYB domain (Figs 1c, S1b; Raxwal *et al.*, 2020). At 20°C, the FS(.1) transcript accumulates at low levels, with the RVE2 _ID2 isoform predominating (Fig. 1d,e; Calixto *et al.*, 2018). However, after chilling, the FS(.1) isoform begins to increase within 20 min (Fig. 1d), with this transition between the _ID2 and FS(.1) isoforms persisting for several days after transfer to 4°C (Fig. 1e). Thus, RVE2 undergoes a cold-induced isoform switch involving the FS(.1) and _ID2 isoforms. An alternative splicing isoform switch is where a pair of transcript isoforms reverse their relative expression abundances in response to external or internal stimuli (Sebestyén *et al.*, 2015; Guo *et al.*, 2017). To validate the reversal of relative isoform expression, we performed isoform specific qRT-PCR for time points immediately after the onset of cooling (Fig. S1b,c). These data confirm the rapid cold-induced alternative splicing of RVE2; transcripts containing the premature stop codon were

significantly lower after only 15 min of cooling ($P = 0.0004$), whereas FS(.1) was higher after 60 min of cooling ($P = < 0.0001$; Fig. S1c).

We next quantified how chilling alters the population of RVE2 alternately spliced isoforms (Fig. 1f). Before chilling, the FS(.1) isoform constitutes only 4.5% of the total RVE2 expression, whereas _ID2 comprises 81% (ZT18, Fig. 1f, Shannon diversity index = 0.77). Chilling alters RVE2 alternative splicing and increases the proportion of FS(.1) to 92.1% of expressed transcripts 6 h after chilling (ZT18, Fig. 1f, Shannon diversity index = 0.38; $P < 0.001$). Following an extended period of cooling, peak RVE2 expression is damped but FS(.1) remains the major component at 81% (ZT18, 78 h after chilling, Fig. 1e,f, Shannon diversity index = 0.75). The _ID1 isoform (which encodes a 4 AA peptide; Fig. 1c), was evident in the 20°C and 4°C acclimated peaks, albeit at low levels (8.0% and 6.9%, respectively, Fig. 1f) and therefore the RVE2 transcript primarily featured altered abundance of the FS(.1) and _ID2 isoforms after chilling (Fig. 1f).

RVE2 alternative splicing is proportional to temperature changes and continues in constant light

Alternative splicing is affected by both temperature and light (Martín *et al.*, 2021). Since RVE2 alternative splicing was observed within 20 min (after ambient temperature had reached 16°C; Fig. 1d), we were interested whether alternative splicing of RVE2 was affected by the magnitude of chilling applied and whether the patterns of alternative splicing observed were maintained in constantly lit conditions (Fig. 2). We first used qRT-PCR to examine alternative splicing after transfer to different temperatures (Fig. 2a). In addition to 4°C, RVE2 alternative splicing was induced when plants were chilled to either 12°C or 8°C with the proportion of RVE2 FS(.1) increasing as temperatures decreased (Fig. 2a). These data suggest that RVE2 alternative splicing is sensitive to the magnitude of chilling experienced.

RVE2 was expressed with a daily pattern (Fig. 1e) and so we next examined how RVE2 expression and alternative splicing were affected when held in constantly lit conditions. Since the circadian system is damped when held at low temperatures for

Fig. 1 RNA-seq reveals altered patterns of alternative splicing during chilling. (a) Differential gene expression (DE) and differential alternative splicing (DAS) were examined in *Arabidopsis thaliana* for a high-resolution RNA-seq time-series across the first 3 h of cooling. Data are plotted when each gene was first significantly DE or DAS (each gene is represented only once). (b) Relationship between Δ alternately spliced (ΔAS) and expression level (TPM) for 35 k transcripts for genes expressing at least two transcripts (Supporting Information Dataset S2). Red circle denotes *RVE*2 FS(.1). (c) Diversity of *RVE2* transcripts. Transcript maps of seven alternatively spliced *RVE2* transcripts identified using AtRTD2-QUASI (Zhang *et al.*, 2017). Transcript maps: white boxes – coding sequences; black boxes – UTRs; gray box – intron retention. Where an AS event causes introduction of a premature stop codon and loss of open reading frame, the downstream region is represented by black boxes (UTRs). (d) *RVE2* cold-induced alternative splicing of the FS(.1) and _ID2 isoforms for the first 3 h after dusk, either for plants experiencing no cooling (*left*, steady state 20°C), or for plants subjected to cooling (*right*, cooling to 4°C). Temperature bar (top) indicates growth cabinet temperature at the denoted time points. (e) Temperature and diel time series describing *RVE2* isoform accumulation (mean ± SE (*n* = 3)). Data are plotted relative to the initiation of chilling to 4°C (dashed blue vertical line), diurnal 12 h : 12 h, dark : light conditions denoted by black/white rectangles, respectively. (f) Stacked bar representation of % abundance of denoted isoforms at 20°C at ZT18 (before cooling), at ZT18 during cooling, and at ZT18 on the fourth day after cooling, 78 h after the initiation of chilling. Total TPM for time points is denoted above the stacked bars, representative abundances (%) denoted within bars or to side of bars. Diversity of transcript isoforms at each time point is quantified using the Shannon Index, with error bars denoting 95% confidence intervals. '***' indicates $P < 0.001$.
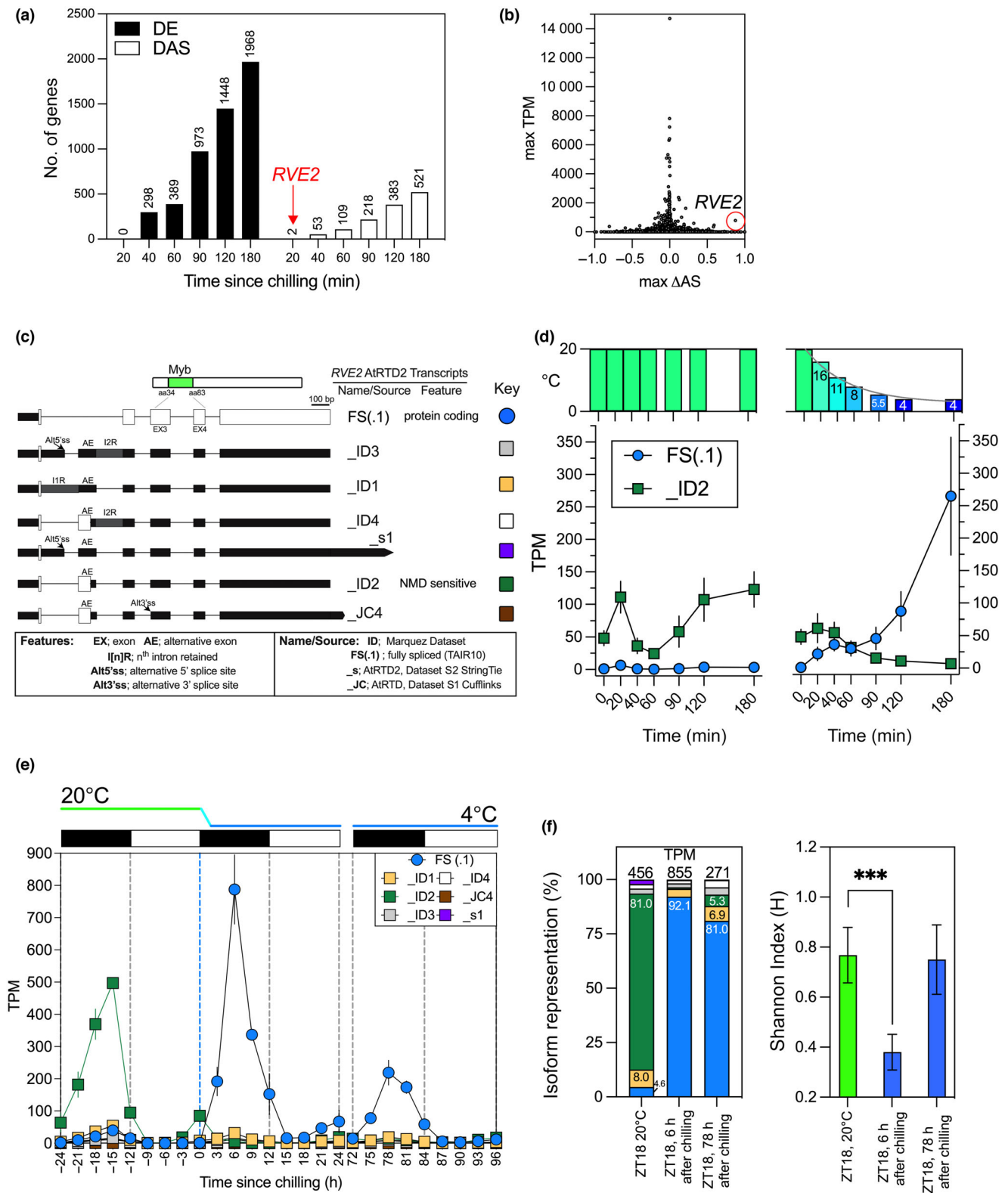
prolonged periods, we chose to chill to 12°C under constant light to maintain rhythmic gene expression (Fig. 2b–h; Dataset S3; Ramos *et al.*, 2005; Bieniawska *et al.*, 2008). Consistent with our experiments under driven light : dark cycles, FS(.1) *RVE2* is a minor constitutent at 20°C under constant light (LL; Fig. 2b,c), whereas the _ID2 isoform maintained a robust, higher amplitude rhythm in 20°C LL (Fig. 2b,d). When chilled to 12°C at ZT12, FS(.1) *RVE2* displayed circadian rhythms of accumulation

(Fig. 2b,c). Circadian patterns of accumulation were also observed for _ID2, albeit with reduced amplitude (Fig. 2d). Comparable data were obtained using isoform-specific RT-qPCR (Fig. S2). By contrast, the _ID1 and _ID4 *RVE2* isoforms were less affected by chilling, although we did observe a delayed pattern of accumulation in both isoforms when held at 12°C (Fig. 2e,f). In general, plants held in constant light at 12°C generated a much more diverse population of *RVE2* transcripts compared to those chilled to 4°C in light : dark cycles (Figs 1f, 2g,h). These changes reflect the responsiveness of *RVE2* alternative splicing to environmental factors that could be caused by a combination of light and temperature signals.

Disruption of *RVE2* alternative splicing alters differential gene expression in response to chilling

We wanted to determine the biological relevance of *RVE2* alternative splicing. The previously reported *rve2-1* allele still accumulated the 5′ portion of the FS(.1) transcript in response to chilling when assessed using qRT-PCR, suggesting that cold-induced alternative splicing still occurs in this allele (Fig. S3a; Zhang *et al.*, 2007). We therefore identified an additional Col-0 T-DNA insertional mutant (GABI-Kat 508D10, *rve2-2*), harboring the insertion in the alternative exon within the first intron of the *RVE2* gene (Figs 3a, S3a). Homozygous mutants were verified by diagnostic PCR using *RVE2*-specific and T-DNA border primers (Fig. S3b,c), and by assessing sensitivity to sulfadiazine (Fig. S3d). qRT-PCR confirmed the absence of the cold-induced induction of FS(.1) *RVE2 in rve2-2* across our time course (Fig. S3e,f).

We next performed RNA-seq on rosettes of 5-wk-old Arabidopsis Col-0 and *rve2-2* plants for biological replicates of a diurnal, temperature, and time-series experiment to assess the role of RVE2 in cold responses (Fig. 3; Dataset S4). Consistent with our initial PCR analysis (Fig. S3), RNA-seq reads mapped to the *RVE2* FS(.1) and _ID2 isoform models for Col-0, but not for *rve2-2*, confirming the loss of *RVE2* gene expression in *rve2-2* (Fig. 3a). Although reads mapped to the other *RVE2* isoform models (Fig. S4), their levels in *rve2-2* were much lower than Col-0, except for the _ID1 and _ID4 isoforms (Fig. S4a,c, respectively), which encode greatly truncated proteins (Fig. 1c).

Our comprehensive RNAseq dataset allowed completion of a differential trend analysis to assess whether genes beyond *RVE2* were constitutively misregulated in *rve2-2* seedlings. The analysis identified transcript isoforms that exhibited significant differences in expression trends, based on an adjusted *P*-value threshold of < 0.01 (Guo *et al.*, 2021). Among the transcripts, only two genes (*RVE2* and the uncharacterized AT5G27390) were found to have individual transcript isoforms with expression reduction of > 2 TPM (Figs S4, S5). However, *RVE2* was the only gene that demonstrated a reduction in gene-level expression in the *rve2-2* samples (Figs S4a, S5a). This analysis is consistent with a single T-DNA insertion within the *RVE2* locus for the *rve2-2* allele.

In order to evaluate the induction of productive FS(.1) *RVE2* splicing, we generated transgenic lines expressing a RVE2:LUC translational fusion in the *rve2-2* background (Fig. 3b). Since chilling to 4°C impairs luciferase activity (Rabha *et al.*, 2021), we assessed RVE2:LUC bioluminescence following chilling to 12°C. While quantitative comparisons of luciferase activity at different temperatures are limited by the lability of the enzyme, RVE2:LUC bioluminescence increased following chilling, peaking *c.* 8 h after dusk (Fig. 3b). Luciferase activity was reduced from the following dawn despite maintaining the lower temperature, likely due to reduced accumulation of *RVE2* FS(.1) (Fig. 1e). Following return to 20°C, bioluminescence returned to their original levels although distinct patterns of luciferase activity remained (Fig. 3b). These data suggest that FS(.1) RVE2 accumulation increases due to the coincidence of *RVE2* expression and reduced temperatures.

Chilling has previously been reported to induce alternative splicing of two other *RVE* family members, *CCA1* and *LHY* (Seo *et al.*, 2012; James *et al.*, 2012, 2018). Our dataset reproduces the reported changes in *CCA1* and *LHY*, although the alternative splicing begins *c.* 3 h later than the events identified in *RVE2* (Figs 3a,c,d, S6; Dataset S4). Our data also reveal alternative splicing of *RVE8* in response to chilling, although splicing is unaffected in other *RVE* gene products (Fig. S6). However, each of these differential splicing events were maintained in the *rve2-2* background, suggesting that RVE2 itself does not contribute to alternative splicing in response to chilling (Figs 3c,d, S7; Dataset S4).

As *rve2-2* lines retain expression and alternative splicing of other *RVE* family members, we next examined whether *rve2-1* and *rve2-2* had a circadian phenotype using seedlings expressing a *CCA1::LUC2* reporter (Fig. 3e–h). When held at 20°C under

Fig. 2 Alternative Splicing of RVE2 persists in free-run conditions. (a) Alternative splicing of *RVE2* in plants undergoing different extents of cooling was examined using RT-qPCR, *upper* FS(.1) isoform and *lower* AE isoform. Plants were entrained in 20°C in LD cycles before transfer to the denoted temperature at dusk. The $\Delta\Delta C_t$ method was used to calibrate normalized Ct values (using the average of Cts for *IPP2* and *ISU1* housekeeping genes) to the time point demonstrating maximal expression. (b) Accumulation of *RVE2* alternatively spliced isoforms in constant light at either 20°C or 12°C by RNA-seq. Col-0 plants were grown to maturity (5 wk) in 12 h : 12 h, dark : light at 20°C, then either held at 20°C or chilled to 12°C at ZT12 in constant light. Subjective dark phases are denoted using light-gray shaded boxes. Plants were harvested every 4 h, except an additional time point at ZT18 (6 h after chilling). (c–f) Comparison of 20°C and 12°C *RVE2* isoform expression profiles for (c) FS(.1); (d) _ID2; (e) _ID1 and (f) _ID4. Data are normalized mean and ± SE (*n* = 3) of expression levels (TPM; transcripts per million). (g) Stacked bar representation of % abundance of isoforms (TPM levels) at ZT18 at 20°C or 12°C (6 h after chilling). Total TPM for peaks presented above the stacked bars, with % abundances denoted within bars. (h) Diversity of transcript isoforms at these selected time points was quantified using the Shannon Index, with error bars denoting 95% confidence intervals. '***' indicates *P* < 0.001.
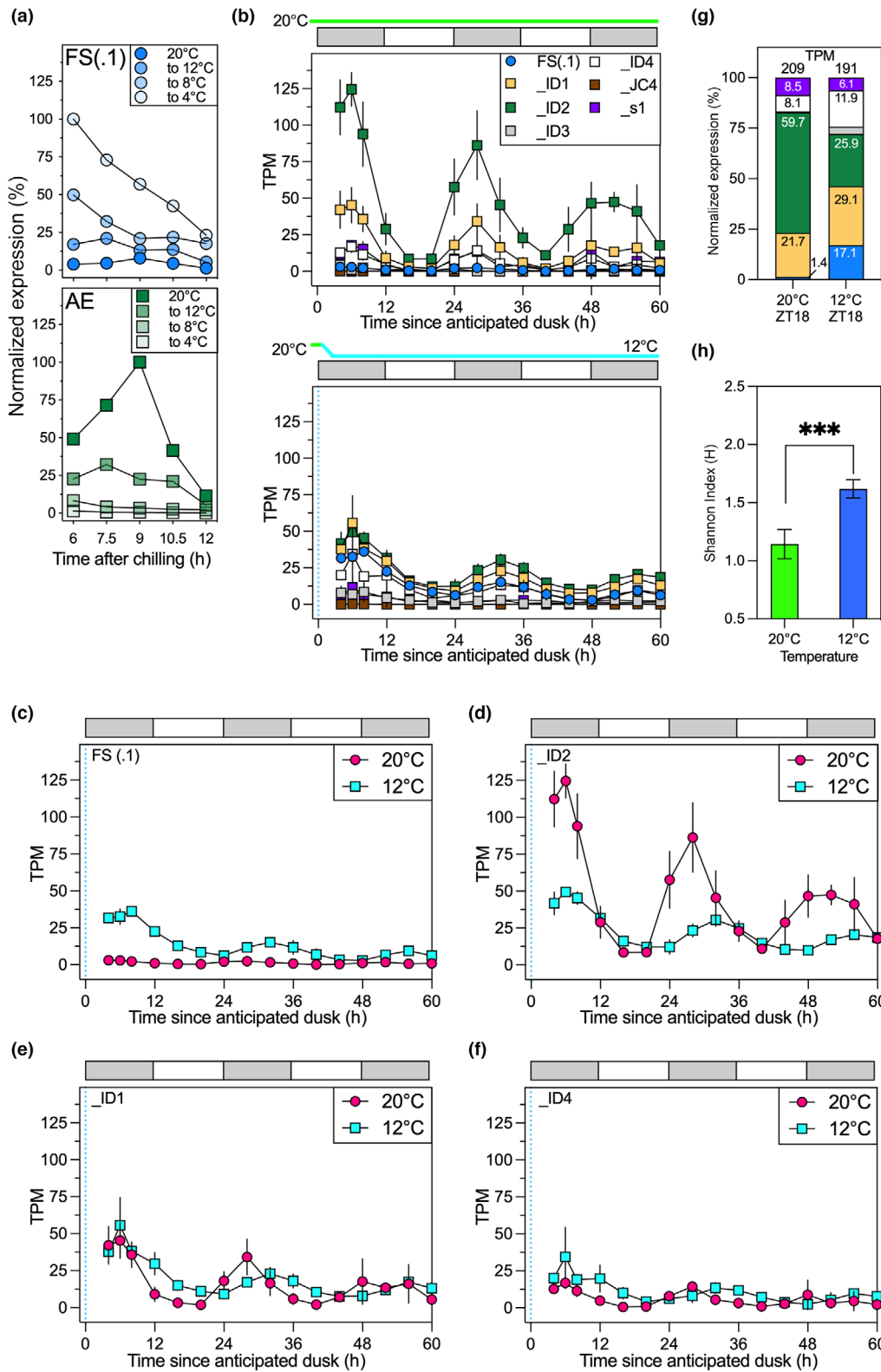
constant white light, *rve2-1* seedlings were indistinguishable from wild-type ($P = 0.723$, Dunnett's multiple comparisons test), whereas *rve2-2* seedlings had a modestly extended circadian period (+0.32 h, $P = 0.02$, Dunnett's multiple comparisons test; Fig. 3e,f). Chilling to 12°C induced a greater difference in circadian period between wild-type and *rve2-2* seedlings at reduced

temperatures (+1.1 h, $P < 0.01$) although *rve2-1* seedlings remained indistinguishable from the control ($P = 0.338$; Fig. 3g, h). These data suggest that RVE2 contributes to the maintenance of circadian rhythms at lower temperatures and that *rve2-2* is a stronger allele with regard to the circadian mutant phenotype observed.
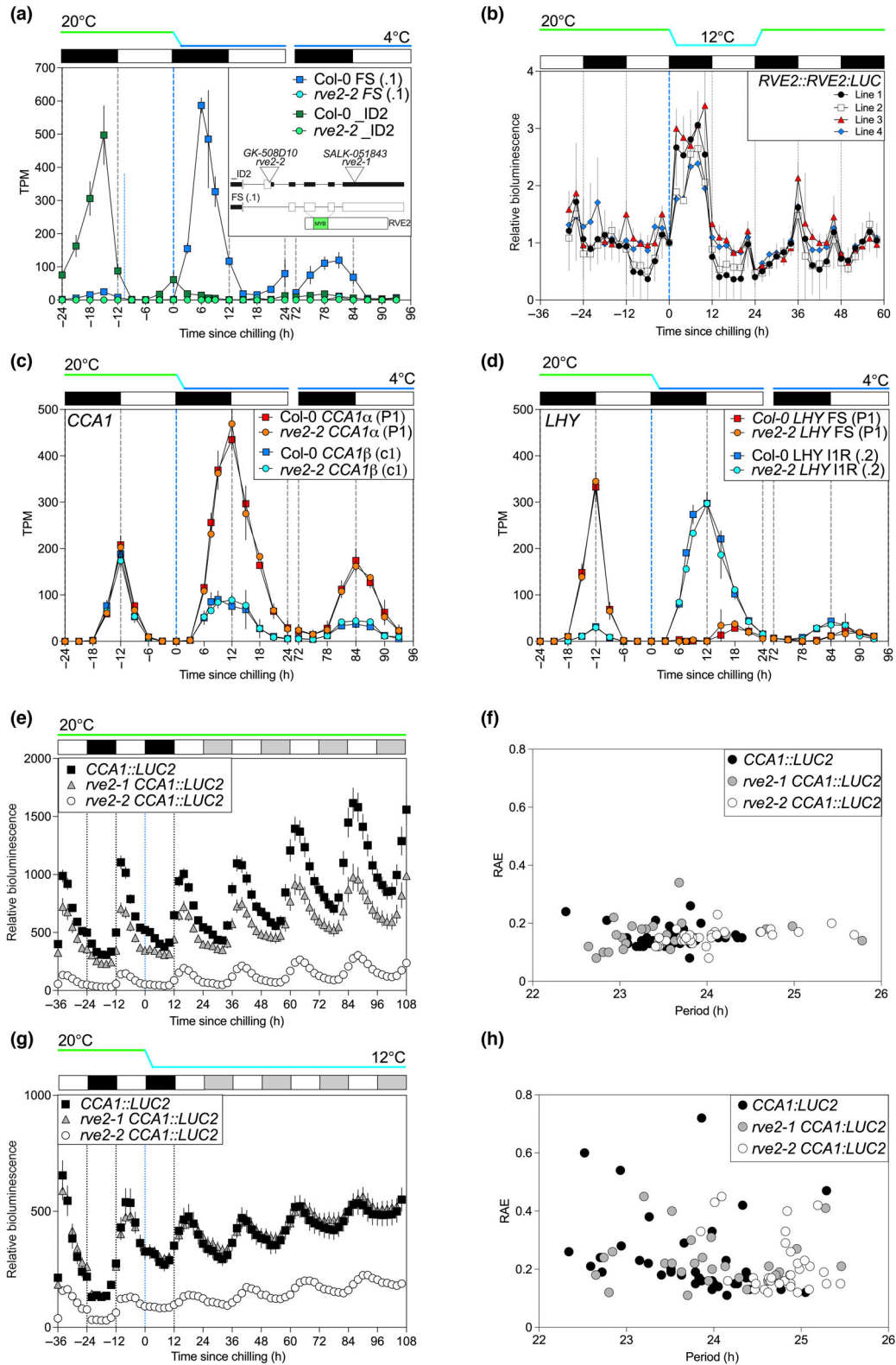
Fig. 3 Assessment of circadian phenotypes in *rve2* seedlings (a) Accumulation of *RVE2* FS(.1) and *RVE2* _ID2 isoforms in Col-0 and *rve2-2* seedlings before, during, and after chilling to 4°C. Col-0 plants were grown to maturity (5 wk) in 12 h : 12 h, dark : light at 20°C, then either held at 20°C or chilled to 4°C at ZT12. Plants were harvested every 3 h, except an additional time point 7.5 h after chilling. The insert shows the T-DNA insertion site of Gabi-Kat line 508D10 within the first intron of *RVE2* compared to the previously identified *rve2-1* (Zhang *et al.*, 2007). The predominant FS(.1) and _ID2 isoforms are illustrated, with white boxes indicating translated exons. Black boxes show untranslated sequence due to the inclusion of a premature stop codon. The sequence encoding the conserved MYB domain in the FS protein is indicated in green. (b) Bioluminescence recorded from seedlings expressing a *RVE2::RVE2:LUC* fusion reporter in a *rve2-2* background at different temperatures. Data are shown from four independent transgenic lines and indicates luciferase activity derived from the fully-spliced RVE2:LUC fusion protein relative to the dusk time point immediately before chilling. (c) Accumulation of *CCA1α* (fully spliced) and *CCA1β* isoforms in Col-0 and *rve2-2* seedlings before, during, and after chilling to 4°C. Data were taken from the experiment described in (a). (d) Accumulation of *LHY* (P1, fully-spliced) and *LHY 0*.2 (I1R, Intron 1 retained) isoforms in Col-0 and *rve2-2* seedlings before, during and after chilling to 4°C. Data were taken from the experiment described in (a). (e) Patterns of luciferase bioluminescence in wild-type, *rve2-1*, and *rve2-2* seedlings in plants expressing a *CCA1::LUC2* reporter held in constant white light at 20°C. (f) Circadian period estimates based on data presented in (e). (g) Patterns of luciferase bioluminescence in wild type, *rve2-1*, and *rve2-2* seedlings in plants expressing a *CCA1::LUC2* reporter held in constant white light following chilling to 12°C at dusk. (h) Circadian period estimates based on data presented in (g). Cooling was initiated at dusk, white and black bars indicate 12 h light and dark periods, respectively. Subjective dark periods in constant light are indicated with shaded gray bars. All error bars represent ±SE of the mean.

Transcriptome sequencing reveals that *rve2* plants have altered gene expression in the 12 h immediately after the initiation of chilling

We reasoned that differences in expression between Col-0 and *rve2-2* would be most noticeable at, or soon after, the onset of chilling and so compared transcript accumulation during the 24 h after temperature reduction. After filtering out low expressed isoforms (discarding isoforms with a sum TPM < 80 across the Day 2 time points), we identified isoforms showing consistent Differential Expression (DE) for three consecutive time points. This approach provided seven consecutive DE bins across the 24 h period after chilling, namely h0-6 (i.e. the points at h0, 3 and 6), h3-9, h6-12, h9-15, h12-18, h15-21, and h18-24 (Fig. 4a). Candidate isoforms were also split into two categories: those that showed consistent DE where *rve2-2* TPM levels were higher than Col-0 (up-regulated) and those that showed *rve2-2* TPM levels lower than Col-0 (downregulated). We found that the number of consistently upregulated isoforms increased during the initial phase of cooling (during the first 15 h after chilling) to reach a peak for the h6-12 bin and then decreased (Fig. 4b). There was a less clear pattern for isoforms downregulated in *rve2-2*, with an initial peak from h6-12 followed by a second peak in the h15-21 bin (Fig. 4c). The identity of the downregulated and upregulated isoforms for the consistent DE bins is provided in Dataset S5.

Our DE analysis of the 24 h after chilling identified 1097 upregulated and 1446 downregulated isoforms (Fig. 4b,c; Dataset S5). Two-way ANOVAs were performed on these upregulated and downregulated candidate isoform lists to assess the effect of genotype (*rve2-2* and Col-0) and timing on isoform expression levels. Around half of the DE candidates were significantly misregulated (P-value ≤ 0.05), resulting in groups of 486 and 643 for upregulated and downregulated DE isoforms, respectively (Dataset S5). These isoforms are encoded by 435 upregulated genes and 619 downregulated genes. The Evening Element (AAAATATCT), which has previously been shown to be bound by RVE family members, is enriched in the promoters of our upregulated group of genes (33%; Michael & McClung, 2002, Harmer & Kay, 2005, Rawat *et al.*, 2009, Heinz *et al.*,

2010). Gene Ontology (GO) term enrichment of these gene loci sets show enrichment for Biological Process terms 'response to cold', 'response to light intensity', 'circadian rhythm' and 'rhythmic process' for the upregulated group and photosynthetic terms for the downregulated group (Fig. 4d).

Previous analysis has used hierarchical clustering of DE genes to reveal groups of transient-, adaptive- and late-expressed genes in response to chilling (Calixto *et al.*, 2018). We aligned our significantly upregulated and downregulated genes with these previously identified clusters and performed one-sided Fisher's exact tests to establish enrichment (Odds Ratios) of genes within cluster groups (Fig. 4e; Dataset S5; Calixto *et al.*, 2018). About 68% of upregulated candidates merged with a cluster group (295 out of 435). Clusters 9, 20, and 25 showed particularly high enrichment of upregulated isoforms (Odds Ratios > 7, Fig. 4e). Membership of these three clusters accounted for 54% of the upregulated group. For the downregulated candidates, *c.* 49% could be assigned to a cluster (302 out of 619). For downregulated genes, cluster 17 was noticeably enriched, accounting for 10% of the downregulated group (Fig. 4e). Fig. 4f contrasts the Col-0 and *rve2-2* mean *z*-score expression profiles for the enriched clusters 9, 20, 25, and 17, and suggest that rapid nocturnal repression and subsequent activation of candidate isoforms is the prominent role for RVE2 immediately after chilling.

Given the circadian phenotype of *rve2-2* seedlings at reduced temperatures, we next assessed the role of RVE2 in regulating candidate gene expression. *rve2-2* plants display altered expression of the *RVE6* _P2 isoform (Fig. 5a, $P = 0.0018$), as well as promoting accumulation of the *PRR5* .1 ($P = 0.019$), and *ELF4* _P1 ($P < 0.0001$) isoforms (Fig. 5b; Dataset S5). Beyond circadian genes, altered expression was found for *CBF3* (Fig. 5c, _JC1 isoform, $P = 0.0074$), *CBF1* (Fig. 5d, .1 isoform, $P = 0.003$), and *CBF2* (Fig. 5e, .1 isoform, $P = 0.0083$). For all three *CBF*s, transcript levels were higher in *rve2-2* than in Col-0 after 6 h of cooling and remained elevated until the following dawn. These differences were particularly concentrated to the first night of cooling since the remainder of the timecourse was virtually indistinguishable between Col-0 and *rve2-2* for these transcripts (Fig. 5; Dataset S4).

Later in the timecourse, we found that all 31 members of Cluster 17 are downregulated in *rve2-2* compared with Col-0 across
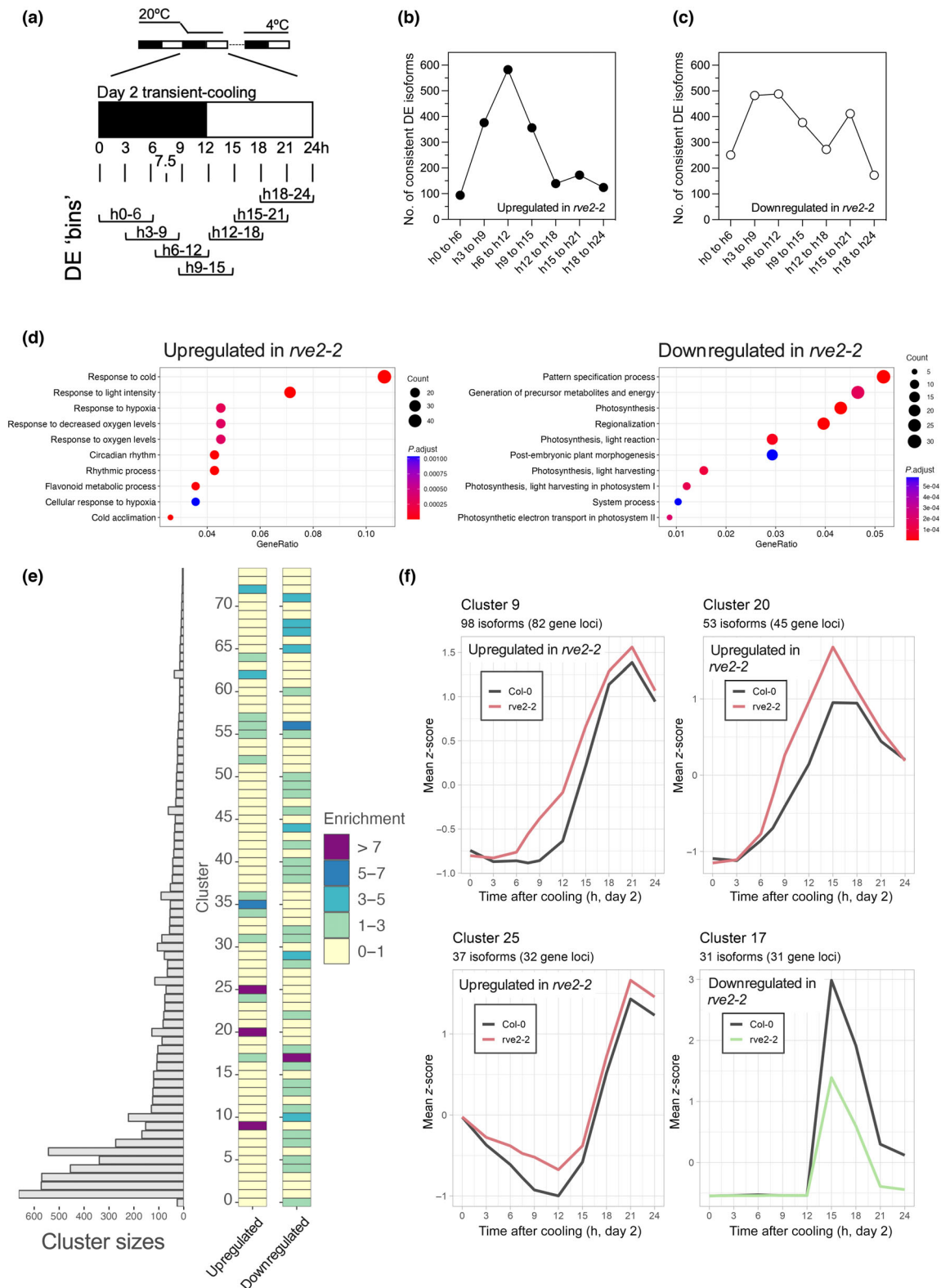
Fig. 4 Disruption of *RVE2* alternative splicing alters gene expression following chilling. (a) Overview of categorization used to identify transcript isoforms consistently differentially expressed in *rve2-2* compared with Col-0 across the transient-cooled Day 2 of the temperature and time series RNA-seq experiment. (b) Transcript isoforms consistently upregulated in *rve2-2* compared to Col-0 in the indicated time frames. (c) Transcript isoforms consistently downregulated in *rve2-2* compared with Col-0 in the indicated timeframes. (d) Gene Ontology term enrichment plots for biological process for the 'up-regulated in *rve2-2*' (left) and 'down-regulated in *rve2-2*' (right) differentially expressed groups. (e) Alignment and enrichment (Odds ratios) of the grouped h0-24 repressed and activated isoform cohorts with the Calixto *et al.* (2018) TF-cluster groups. (f) Mean *z*-score of *rve2-2* and Col-0 expression plots for differentially expressed genes in the denoted enriched cluster groups.
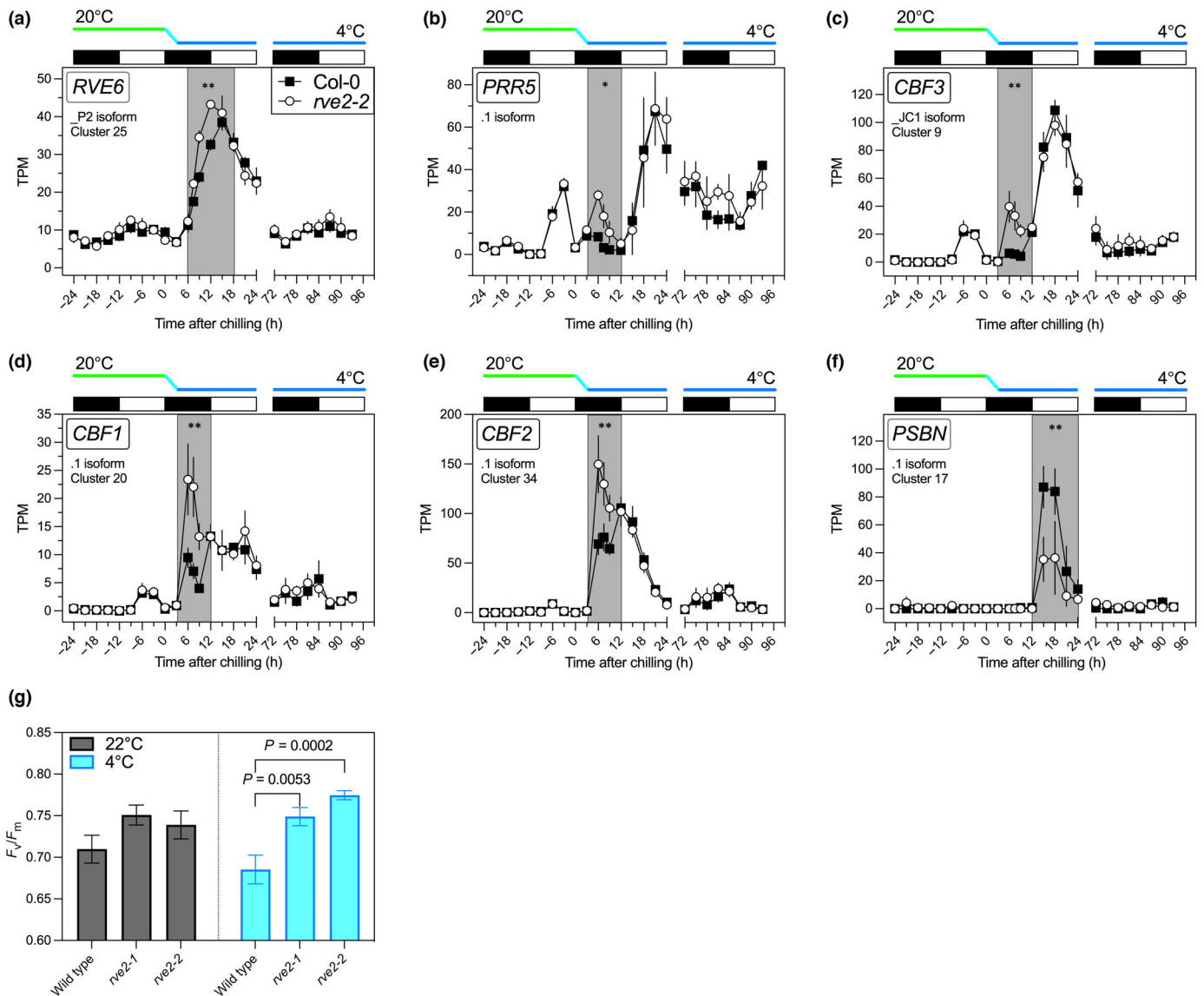
Fig. 5 Altered expression of candidate transcripts in *rve2-2* during the onset of cooling. Temperature and time-series transcript expression plots for a selection of candidate isoforms displaying altered expression in *rve2-2* compared with Col-0. (a) *REVEILLE 6/RVE6* _P2, (b) *PSEUDO-RESPONSE REGULATOR 5/PRR5* .1 (c) *C-REPEAT BINDING FACTOR 3* _JC1, (d) *C-REPEAT BINDING FACTOR 1/CBF1* .1 isoform, (e) *C-REPEAT BINDING FACTOR 2/CBF2* .1 and (f) *PHOTOSYSTEM II REACTION CENTER PROTEIN N/PSBN* .1 (g) Maximum quantum efficiency of PSII photochemistry of Col-0, *rve2-1*, and *rve2-2* seedlings before and after cool night chilling. For (a – f), data represent TPM mean ± SE ($n = 3$). Alternating black–white rectangles denote 12 h dark–light phases, respectively. Cluster designations correspond with Fig. 4. Data are presented relative to the onset of chilling at dusk. Two-way ANOVA P-value summary statistic is highlighted for time points with differential gene expression (*, $P < 0.05$; **, $P < 0.01$).

the first photoperiod after chilling (Fig. 4f). These Cluster 17 genes are all chloroplast-encoded and include *PHOTOSYSTEM II REACTION CENTER PROTEIN N* (*PSBN*, Fig. 5f, .1 isoform, $P = 0.01$). The expression profiles for all other chloroplast-encoded candidate genes were broadly similar with a pulse of expression after dawn in the photoperiod of Day 2 'transient', with expression maxima 3 h after dawn. We hypothesized that the differences in gene expression observed would culminate in altered photosynthetic performance, and so measured the maximum quantum efficiency of PSII photochemistry (F_v/F_m) in plants either maintained at 22°C or chilled overnight at 4°C (Fig. 5g). We were interested to observe that in both *rve2-1* and

rve2-2, photosynthetic capacity was significantly higher than wild-type plants following chilling ($P < 0.01$, Tukey's multiple comparison test; Fig. 5g). Such data suggest that RVE2 serves to limit photosynthetic performance at reduced temperatures.

Discussion

Deep sequencing reveals chilling-induced alternative splicing of *RVE2* pre-mRNA

For plants, timing is everything. The alternative splicing of *RVE2* offers the opportunity to understand how plants perceive and

integrate overnight chilling signals. *RVE2* alternative splicing occurs almost simultaneously with cooling and the immediacy of this response strongly suggests a mechanism centered on thermo-sensitive splicing (Figs 1, S1). The rapid and substantial induction of *RVE2* alternative splicing and the altered accumulation of *CBF* transcripts in *rve2-2* plants similarly suggest that RVE2 splicing comprises an early actor in the response to chilling (Figs 1d, 5). Although some aspects of *RVE2* differential expression and alternative splicing have previously been described (Filichkin & Mockler, 2012; Filichkin *et al.*, 2015), the functional transition between different protein-coding isoforms has until now remained hidden. We suggest there are two main reasons for this. First, we show that only a small proportion of *RVE2* gene expression produces the canonical FS(.1) RVE2 transcript at ambient temperature and therefore studies characterizing *RVE2* (including phenotypic studies of adult *rve2* plants) at standard ambient temperatures are rendered largely redundant. Second, the detection of *RVE2* chilling-induced splicing was only made possible by transcript-specific RNA-seq analysis – microarray or gene-level RNA-seq analyses would not reveal this response. Transcript-specific RNA-seq analyses relies upon employment of a high-quality, nonredundant reference transcript datasets that distinguish diverse transcript assemblies. Since the TAIR10 reference transcriptome contains only a single *RVE2* transcript, previous studies examining temperature-dependent alternative splicing could not distinguish the *RVE2* AS isoforms (e.g. Romanowski *et al.*, 2020; Bonnot & Nagel, 2021). By contrast, we employed an alternative transcriptome reference that recognizes seven *RVE2* transcript isoforms (AtRTD2; Zhang *et al.*, 2017). Most of the differences between these isoforms are due to splice site choice in the first intron (Fig. 1c). Two of the isoforms, _ID2 (containing an alternative exon in intron 1, introducing a premature termination codon), and the protein coding FS(.1), make up over 85% of *RVE2* transcripts generated, with the proportion of these changing dependent upon temperature (Fig. 1f). Additional work will be required to fully understand the mechanism underlying *RVE2* alternative splicing.

Chilling-induced alternative splicing of RVE family members *CCA1* and *LHY* has previously been reported in addition to *RVE2*, although the consequences for protein function appear to be distinct in each case (Seo *et al.*, 2012; James *et al.*, 2018). Low temperatures restrict accumulation of *CCA1β*, which encodes a truncated protein lacking the DNA-binding Myb domain (Fig. 3c; Seo *et al.*, 2012; Zhang *et al.*, 2021). It has previously been suggested that the truncated *CCA1β* restricts full-length *CCA1α* function via heterodimerization and impaired DNA binding, possibly by retaining *CCA1α* in the cytosol (Seo *et al.*, 2012; Zhang *et al.*, 2021). By contrast, alternative splicing within the *LHY* 5′ UTR does not alter the encoded protein but may instead enhance RNA stability to indirectly promote LHY accumulation (James *et al.*, 2018). *RVE2* alternative splicing produces two primary transcripts, *RVE2* FS(.1) and *RVE2* _ID2 (Fig. 1c). Unlike *CCA1β*, *RVE2* _ID2 does not encode substantial proteins from alternate start sites, with the longest predicted peptide consisting of 23 amino acids that lacks homology to the RVE2 FS(.1) protein. Therefore, although alternative splicing of

CCA1, *LHY*, and *RVE2* is expected to increase the biological activity of each protein the underlying mechanism is distinct, with the transcript encoding *RVE2* FS(.1) accumulating as temperatures decrease (Fig. 3b). Work examining plants over-expressing *RVE2* cDNA (i.e. FS(.1)) can be re-interpreted in the context of the cold-induced isoform described here (Zhang *et al.*, 2007; Guan *et al.*, 2013).

RVE2 alternative splicing provides a mechanism to integrate lower night-time temperatures with the circadian system

RVE2 has not previously been regarded as contributing to circadian clock function, likely because classical mutagenic screens for circadian mutants were completed *c*. 22°C where the *RVE2* _ID2 isoform predominates (Fig. 1; Millar *et al.*, 1995). We used a clock promoter fused to luciferase (*CCA1::LUC2*) to establish a circadian phenotype for the *rve2-2* allele showing that RVE2 contributes to circadian timing at reduced temperatures (Fig. 3). The FS(.1) isoform continues to be expressed at 20°C, although it is also possible that _ID2 produces a protein that alters circadian rhythms (Fig. 3). The absence of a circadian mutant phenotype in *rve2-1* seedlings could arise from the retention of temperature-sensitive alternative splicing in this mutant background and highlights the relative importance of the conserved MYB-domain for circadian function (Figs 3, S3).

Potential RVE2 targets were identified using RNA-seq comparing Col-0 and *rve2-2* plants (Figs 4, 5; Dataset S5). Genes misregulated in *rve2-2* plants typically responded to chilling within the first 6–12 h after chilling (Figs 4, 5), concurrently with the accumulation of a RVE2:LUC fusion protein (Figs 3b, 4b). Our data are consistent with RVE2 serving predominantly as a transcriptional repressor, as observed for other RVE family members which each contain a single Myb-like domain (Figs 4, 5; Gray *et al.*, 2017). Our data demonstrate that cold-induced activation of *CBF* expression is enhanced in *rve2-2* plants after chilling at dusk, suggesting that RVE2 restricts their expression (Fig. 5; Table S2). This effect contrasts with CCA1- and LHY-mediated activation of *CBF* expression after dawn-phased chilling, suggesting that RVE2 works with alternate cofactors to regulate gene expression (Dong *et al.*, 2011). The different contributions of CCA1, LHY, and RVE2 to govern *CBF* induction at different times of day suggest a mechanism to enable time-of-day-dependent responses to chilling.

While temperature as an environmental signal is notoriously difficult to isolate (since temperature affects nearly all biological processes; Wang *et al.*, 2022), the activity of RVE2 after dusk could contribute to circadian gating of the temperature response overnight. Beyond nightly cooling, temperature-dependent splicing of *RVE2* also enables the integration of seasonal information into the circadian system. We would expect greater RVE2 accumulation during the cooler nights experienced during the winter, and it will be interesting to learn if the interplay between temperature, daylength, and light intensity influences *RVE2* FS(.1) expression and cold response gating.

Acknowledgements

Competing interests

None declared.

Author contributions

ABJ, JWSB, RZ, HGN and MAJ planned and designed the research. ABJ, CS, JL, EMA, NT and MAJ performed experiments. ABJ, CS, WG, RZ and MAJ analyzed data. ABJ, HGN and MAJ wrote the manuscript with help from all authors.

ORCID

Emily May Armstrong https://orcid.org/0000-0002-8342-1489
John W. S. Brown https://orcid.org/0000-0003-2979-779X
Wenbin Guo https://orcid.org/0000-0002-1829-6044
Allan B. James https://orcid.org/0000-0003-4472-7095
Matthew A. Jones https://orcid.org/0000-0002-3943-3968
Janet Laird https://orcid.org/0000-0002-3290-7577
Hugh G. Nimmo https://orcid.org/0000-0003-1389-7147
Chantal Sharples https://orcid.org/0000-0002-3141-6848
Nikoleta Tzioutziou https://orcid.org/0000-0002-5041-0513
Runxuan Zhang https://orcid.org/0000-0001-7558-765X

Data availability

The data that support the findings of this study are available in the NCBI Sequence Read Archive (SRA) at https://www.ncbi.nlm.nih.gov/sra, reference nos. PRJNA909847, PRJNA909639, and PRJNA1028490.

References

Battle MW, Jones MA. 2020. Cryptochromes integrate green light signals into the circadian system. *Plant, Cell & Environment* 43: 16–27.

Bieniawska Z, Espinoza C, Schlereth A, Sulpice R, Hincha DK, Hannah MA. 2008. Disruption of the Arabidopsis circadian clock is responsible for extensive variation in the cold-responsive transcriptome. *Plant Physiology* 147: 263–279.

Bonnot T, Nagel DH. 2021. Time of the day prioritizes the pool of translating mRNAs in response to heat stress. *Plant Cell* 33: 2164–2182.

Boyle EI, Weng S, Gollub J, Jin H, Botstein D, Cherry JM, Sherlock G. 2004. GO::TermFinder–open source software for accessing Gene Ontology information and finding significantly enriched Gene Ontology terms associated with a list of genes. *Bioinformatics* 20: 3710–3715.

Calixto CPG, Guo W, James AB, Tzioutziou NA, Entizne JC, Panter PE, Knight H, Nimmo HG, Zhang R, Brown JWS. 2018. Rapid and dynamic alternative splicing impacts the Arabidopsis cold response transcriptome. *Plant Cell* 30: 1424–1444.

Chinnusamy V, Zhu J, Zhu JK. 2007. Cold stress regulation of gene expression in plants. *Trends in Plant Science* 12: 444–451.

Clough S, Bent A. 1998. Floral dip: a simplified method for *Agrobacterium*-mediated transformation of *Arabidopsis thaliana*. *The Plant Journal* 16: 735–743.

Dong MA, Farre EM, Thomashow MF. 2011. Circadian clock-associated 1 and late elongated hypocotyl regulate expression of the C-repeat binding factor (CBF) pathway in Arabidopsis. *Proceedings of the National Academy of Sciences, USA* 108: 7241–7246.

Edelstein AD, Tsuchida MA, Amodaj N, Pinkard H, Vale RD, Stuurman N. 2014. Advanced methods of microscope control using μMANAGER software. *Journal of Biological Methods* 1: e10.

Farinas B, Mas P. 2011. Functional implication of the MYB transcription factor RVE8/LCL5 in the circadian control of histone acetylation. *The Plant Journal* 66: 318–329.

Filichkin SA, Cumbie JS, Dharmawardhana P, Jaiswal P, Chang JH, Palusa SG, Reddy AS, Megraw M, Mockler TC. 2015. Environmental stresses modulate abundance and timing of alternatively spliced circadian transcripts in Arabidopsis. *Molecular Plant* 8: 207–227.

Filichkin SA, Mockler TC. 2012. Unproductive alternative splicing and nonsense mRNAs: a widespread phenomenon among plant circadian clock genes. *Biology Direct* 7: 20.

Fowler S, Thomashow MF. 2002. Arabidopsis transcriptome profiling indicates that multiple regulatory pathways are activated during cold acclimation in addition to the CBF cold response pathway. *Plant Cell* 14: 1675–1690.

Fowler SG, Cook D, Thomashow MF. 2005. Low temperature induction of Arabidopsis *CBF1*, *2*, and *3* is gated by the circadian clock. *Plant Physiology* 137: 961–968.

Gray JA, Shalit-Kaneh A, Chu DN, Hsu PY, Harmer SL. 2017. The REVEILLE clock genes inhibit growth of juvenile and adult plants by control of cell size. *Plant Physiology* 173: 2308–2322.

Green RM, Tobin EM. 1999. Loss of the circadian clock-associated protein 1 in Arabidopsis results in altered clock-regulated gene expression. *Proceedings of the National Academy of Sciences, USA* 96: 4176–4179.

Guan Q, Wu J, Zhang Y, Jiang C, Liu R, Chai C, Zhu J. 2013. A DEAD box RNA helicase is critical for pre-mRNA splicing, cold-responsive gene regulation, and cold tolerance in Arabidopsis. *Plant Cell* 25: 342–356.

Guo W, Calixto CPG, Brown JWS, Zhang R. 2017. TSIS: an R package to infer alternative splicing isoform switches for time-series data. *Bioinformatics* 33: 3308–3310.

Guo W, Tzioutziou NA, Stephen G, Milne I, Calixto CP, Waugh R, Brown JWS, Zhang R. 2021. 3D RNA-Seq: a powerful and flexible tool for rapid and accurate differential expression and alternative splicing analysis of RNA-Seq data for biologists. *RNA Biology* 18: 1574–1587.

Harmer SL, Kay SA. 2005. Positive and negative factors confer phase-specific circadian regulation of transcription in Arabidopsis. *Plant Cell* 17: 1926–1940.

Heinz S, Benner C, Spann N, Bertolino E, Lin YC, Laslo P, Cheng JX, Murre C, Singh H, Glass CK. 2010. Simple combinations of lineage-determining transcription factors prime *cis*-regulatory elements required for macrophage and B cell identities. *Molecular Cell* 38: 576–589.

Hsu PY, Devisetty UK, Harmer SL. 2013. Accurate timekeeping is controlled by a cycling activator in Arabidopsis. *eLife* 2: e00473.

Hutcheson K. 1970. A test for comparing diversities based on the Shannon formula. *Journal of Theoretical Biology* 29: 151–154.

James AB, Calixto CPG, Tzioutziou NA, Guo W, Zhang R, Simpson CG, Jiang W, Nimmo GA, Brown JWS, Nimmo HG. 2018. How does temperature affect splicing events? Isoform switching of splicing factors regulates splicing of LATE ELONGATED HYPOCOTYL (LHY). *Plant, Cell & Environment* 41: 1539–1550.

James AB, Syed NH, Bordage S, Marshall J, Nimmo GA, Jenkins GI, Herzyk P, Brown JWS, Nimmo HG. 2012. Alternative splicing mediates responses of the Arabidopsis circadian clock to temperature changes. *Plant Cell* 24: 961–981.

Jones MA, Hu W, Litthauer S, Lagarias JC, Harmer SL. 2015. A constitutively active allele of phytochrome B maintains circadian robustness in the absence of light. *Plant Physiology* 169: 814–825.

Kerbler SM, Wigge PA. 2023. Temperature sensing in plants. *Annual Review of Plant Biology* 74: 341–366.

Kidokoro S, Hayashi K, Haraguchi H, Ishikawa T, Soma F, Konoura I, Toda S, Mizoi J, Suzuki T, Shinozaki K. 2021. Posttranslational regulation of multiple clock-related transcription factors triggers cold-inducible gene expression in Arabidopsis. *Proceedings of the National Academy of Sciences, USA* **118**: e2021048118.

Kidokoro S, Kim JS, Ishikawa T, Suzuki T, Shinozaki K, Yamaguchi-Shinozaki K. 2020. DREB1A/CBF3 is repressed by transgene-induced DNA methylation in the Arabidopsis ice1-1 mutant. *Plant Cell* **32**: 1035–1048.

Kidokoro S, Konoura I, Soma F, Suzuki T, Miyakawa T, Tanokura M, Shinozaki K, Yamaguchi-Shinozaki K. 2023. Clock-regulated coactivators selectively control gene expression in response to different temperature stress conditions in Arabidopsis. *Proceedings of the National Academy of Sciences, USA* **120**: e2216183120.

Kleinboelting N, Huep G, Kloetgen A, Viehoever P, Weisshaar B. 2012. GABI-Kat SimpleSearch: new features of the *Arabidopsis thaliana* T-DNA mutant database. *Nucleic Acids Research* **40**: D1211–D1215.

Kuno N, Moller SG, Shinomura T, Xu X, Chua NH, Furuya M. 2003. The novel MYB protein EARLY-PHYTOCHROME-RESPONSIVE1 is a component of a slave circadian oscillator in Arabidopsis. *Plant Cell* **15**: 2476–2488.

Litthauer S, Battle MW, Lawson T, Jones MA. 2015. Phototropins maintain robust circadian oscillation of PSII operating efficiency under blue light. *The Plant Journal* **83**: 1034–1045.

Martín G, Márquez Y, Mantica F, Duque P, Irimia M. 2021. Alternative splicing landscapes in *Arabidopsis thaliana* across tissues and stress conditions highlight major functional differences with animals. *Genome Biology* **22**: 35.

Maruyama K, Sakuma Y, Kasuga M, Ito Y, Seki M, Goda H, Shimada Y, Yoshida S, Shinozaki K, Yamaguchi-Shinozaki K. 2004. Identification of cold-inducible downstream genes of the Arabidopsis DREB1A/CBF3 transcriptional factor using two microarray systems. *The Plant Journal* **38**: 982–993.

Michael TP, McClung CR. 2002. Phase-specific circadian clock regulatory elements in Arabidopsis. *Plant Physiology* **130**: 627–638.

Millar AJ. 2016. The intracellular dynamics of circadian clocks reach for the light of ecology and evolution. *Annual Review of Plant Biology* **67**: 595–618.

Millar AJ, Carre IA, Strayer CA, Chua NH, Kay SA. 1995. Circadian clock mutants in Arabidopsis identified by luciferase imaging. *Science* **267**: 1161–1163.

Mizoguchi T, Wheatley K, Hanzawa Y, Wright L, Mizoguchi M, Song HR, Carre IA, Coupland G. 2002. LHY and CCA1 are partially redundant genes required to maintain circadian rhythms in Arabidopsis. *Developmental Cell* **2**: 629–641.

Patro R, Duggal G, Love MI, Irizarry RA, Kingsford C. 2017. Salmon provides fast and bias-aware quantification of transcript expression. *Nature Methods* **14**: 417–419.

Rabha MM, Sharma U, Barua AG. 2021. Light from a firefly at temperatures considerably higher and lower than normal. *Scientific Reports* **11**: 12498.

Ramos A, Perez-Solis E, Ibanez C, Casado R, Collada C, Gomez L, Aragoncillo C, Allona I. 2005. Winter disruption of the circadian clock in chestnut. *Proceedings of the National Academy of Sciences, USA* **102**: 7037–7042.

Rawat R, Schwartz J, Jones MA, Sairanen I, Cheng Y, Andersson CR, Zhao Y, Ljung K, Harmer SL. 2009. REVEILLE1, a Myb-like transcription factor, integrates the circadian clock and auxin pathways. *Proceedings of the National Academy of Sciences, USA* **106**: 16883–16888.

Rawat R, Takahashi N, Hsu PY, Jones MA, Schwartz J, Salemi MR, Phinney BS, Harmer SL. 2011. REVEILLE8 and PSEUDO-REPONSE REGULATOR5 form a negative feedback loop within the Arabidopsis circadian clock. *PLoS Genetics* **7**: e1001350.

Raxwal VK, Simpson CG, Gloggnitzer J, Entizne JC, Guo W, Zhang R, Brown JWS, Riha K. 2020. Nonsense-mediated RNA decay factor UPF1 is critical for posttranscriptional and translational gene regulation in Arabidopsis. *Plant Cell* **32**: 2725–2741.

Romanowski A, Schlaen RG, Perez-Santangelo S, Mancini E, Yanovsky MJ. 2020. Global transcriptome analysis reveals circadian control of splicing events in *Arabidopsis thaliana*. *The Plant Journal* **103**: 889–902.

Schaffer R, Ramsay N, Samach A, Corden S, Putterill J, Carre IA, Coupland G. 1998. The *late elongated hypocotyl* mutation of Arabidopsis disrupts circadian rhythms and the photoperiodic control of flowering. *Cell* **93**: 1219–1229.

Schneider CA, Rasband WS, Eliceiri KW. 2012. NIH IMAGE to IMAGEJ: 25 years of image analysis. *Nature Methods* **9**: 671–675.

Scholl RL, May ST, Ware DH. 2000. Seed and molecular resources for Arabidopsis. *Plant Physiology* **124**: 1477–1480.

Sebestyén E, Zawisza M, Eyras E. 2015. Detection of recurrent alternative splicing switches in tumor samples reveals novel signatures of cancer. *Nucleic Acids Research* **43**: 1345–1356.

Seo PJ, Park M-J, Lim M-H, Kim S-G, Lee M, Baldwin IT, Park C-M. 2012. A self-regulatory circuit of CIRCADIAN CLOCK-ASSOCIATED1 underlies the circadian clock regulation of temperature responses in Arabidopsis. *Plant Cell* **24**: 2427–2442.

Stamm S. 2008. Regulation of alternative splicing by reversible protein phosphorylation. *The Journal of Biological Chemistry* **283**: 1223–1227.

Tzioutziou NA, James AB, Guo W, Calixto CPG, Zhang R, Nimmo HG, Brown JWS. 2022. Experimental design for time-series RNA-Seq analysis of gene expression and alternative splicing. *Methods in Molecular Biology* **2398**: 173–188.

Vogel JT, Zarka DG, Van Buskirk HA, Fowler SG, Thomashow MF. 2005. Roles of the CBF2 and ZAT12 transcription factors in configuring the low temperature transcriptome of Arabidopsis. *The Plant Journal* **41**: 195–211.

Wang S, Steed G, Webb AAR. 2022. Circadian entrainment in Arabidopsis. *Plant Physiology* **190**: 981–993.

Wang ZY, Tobin EM. 1998. Constitutive expression of the CIRCADIAN CLOCK ASSOCIATED 1 (*CCA1*) gene disrupts circadian rhythms and suppresses its own expression. *Cell* **93**: 1207–1217.

Wickham H. 2016. GGPLOT2. *Use R!* doi: [10.1007/978-3-319-24277-4](https://doi.org/10.1007/978-3-319-24277-4).

Yamaguchi-Shinozaki K, Shinozaki K. 1994. A novel *cis*-acting element in an Arabidopsis gene is involved in responsiveness to drought, low-temperature, or high-salt stress. *Plant Cell* **6**: 251–264.

Yu G, Wang LG, Han Y, He QY. 2012. clusterProfiler: an R package for comparing biological themes among gene clusters. *OMICS* **16**: 284–287.

Zhang R, Calixto CPG, Marquez Y, Venhuizen P, Tzioutziou NA, Guo W, Spensley M, Entizne JC, Lewandowska D, ten Have S et al. 2017. A high quality Arabidopsis transcriptome for accurate transcript-level analysis of alternative splicing. *Nucleic Acids Research* **45**: 5061–5073.

Zhang S, Liu H, Yuan L, Li X, Wang L, Xu X, Xie Q. 2021. Recognition of CCA1 alternative protein isoforms during temperature acclimation. *Plant Cell Reports* **40**: 421–432.

Zhang X, Chen Y, Wang ZY, Chen Z, Gu H, Qu LJ. 2007. Constitutive expression of CIR1 (RVE2) affects several circadian-regulated processes and seed germination in Arabidopsis. *The Plant Journal* **51**: 512–525.

Zielinski T, Moore AM, Troup E, Halliday KJ, Millar AJ. 2014. Strengths and limitations of period estimation methods for circadian data. *PLoS ONE* **9**: e96462.

Supporting Information

Additional Supporting Information may be found online in the Supporting Information section at the end of the article.

Dataset S1 Normalized accumulation of transcripts in the 'Immediate-Early' RNA-seq dataset.

Dataset S2 Individual values for alternatively spliced isoforms presented in Fig. 1(b).

Dataset S3 Normalized accumulation of transcripts in the 'cool LL' RNA-seq dataset.

Dataset S4 Normalized accumulation of transcripts in the Col-0/*rve2-2* genotypes during chilling.

Dataset S5 Summary of differentially expressed genes comparing Col-0 to *rve2-2* using Dataset S4.

Fig. S1 Chilling induced alternative splicing.

Fig. S2 Assessment of *RVE2* alternative splicing under constant light.

Fig. S3 Altered expression of RVE2 transcript isoforms in *rve2-1* and *rve2-2* seedlings during onset of cool nights.

Fig. S4 Temperature and diel time series describing RVE2 isoform accumulation in Col-0 and *rve2-2* plants during and after chilling.

Fig. S5 Temperature and diel time series describing AT5G27390 isoform accumulation in Col-0 and *rve2-2* plants during and after chilling.

Fig. S6 Temperature and diel time series describing RVE family isoform accumulation in Col-0 plants during and after chilling.

Fig. S7 Temperature and diel time series describing RVE family isoform accumulation in *rve2-2* plants during and after chilling.

Methods S1 Detailed information regarding RNA-seq datasets.

Table S1 Primers used in this study.

Table S2 Candidate RVE2 target genes showing significant differential expression (Col-0 vs *rve2-2*) during low-temperature transition.

Please note: Wiley is not responsible for the content or functionality of any Supporting Information supplied by the authors. Any queries (other than missing material) should be directed to the *New Phytologist* Central Office.